Computation of Nonlinear Supersonic Potential Flow over Three-Dimensional Surfaces

M. J. Siclari*
Grumman Aerospace Corporation, Bethpage, New York

A fully implicit three-dimensional marching technique is presented for the computation of inviscid supersonic flows. The nonconservative full potential equation is solved on spherical cross-flow planes using standard transonic SLOR techniques. The three-dimensional bow shock is fitted as a boundary with isentropic jump conditions, and embedded shocks are captured. Applications of these techniques are presented for three-dimensional bodies, wings, and wing-body configurations and the computed solutions are compared to experimental pressure data. Zero-lift wave drag calculations are also presented and compared with measurements to evaluate the accuracy of the present techniques.

Introduction

THE importance of predicting nonlinear effects in supersonic flow (i.e., supercritical cross flows, embedded shock waves) has been demonstrated in several past experimental and numerical studies.[1-6] Panel methods that satisfy the linearized potential equation entirely neglect nonlinear effects. Over the past two decades, panel methods in supersonic flow (e.g., Ref. 7) have matured into sophisticated aerodynamic tools capable of treating somewhat arbitrary three-dimensional aircraft geometries. With this new level of sophistication of supersonic panel methods also comes the increasing penalty of user complexity and computational time requirements. Although panel methods will not be replaced in the near future for the treatment of very complex geometries, the pursuit of a nonlinear supersonic method that solves the full potential equation is becoming an attractive supplement to the linearized techniques, with the long-range goal of accurately treating increasingly complex geometry. As full potential solvers become increasingly efficient,[4,8-11] nonlinear codes are becoming competitive with the linearized techniques and may even be more efficient in predicting detailed pressure distributions that require a large number of panels or computational points.

In Ref. 3, an implicit numerical technique was presented to solve the nonconservative full potential equation for conical flows on a conformally mapped grid that uses a Joukowski transformation to resolve the wing leading edge. The assumption of conical similitude reduces the three-dimensional full potential equation to an equation on the spherical cross-flow surface that closely resembles the two-dimensional transonic nonconservative full potential equation. Hence, the numerical techniques used to solve this equation draw heavily on transonic techniques.[12] This method also captures both bow and embedded cross-flow shocks and was shown to be highly successful and efficient for a variety of conical geometries. The use of a spherical coordinate system ameliorates the axial Mach number problem for typical wing geometries, allowing the computation of flows at much lower Mach numbers. The conical flow code (COREL) was used to tailor the design of a high-lift supercritical conically cambered wing (SC3). The design was successful in meeting the design goals, and the experimental data validated the accuracy of the technique.[13] Shankar et al.[10] have also shown considerable success in computing inviscid supersonic conical flow solutions of the conservative full potential equation. A computed conical solution of Ref. 10 was compared to the solution of Ref. 3 and was found to be in excellent agreement.

The success of the nonlinear conical flow methodology led to extending these techniques to include three-dimensional flows. This task was initiated for delta wing geometries and axisymmetric bodies in Ref. 4. The implicit techniques used for solving the conical flow equation were extended to include nonconical flows by implicitly marching on spherical planes and capturing all shocks. In order to treat more arbitrary and highly nonconical geometries it was further found that a bow shock fitting technique would be more appropriate and accurate. In Ref. 9, an implicit isentropic bow shock fitting technique (BSF) was presented for conical and axisymmetric flows. These techniques are extended in the present study to three-dimensional flows with the bow shock isentropically fit as a boundary. Fitting the bow shock eliminates the inaccuracies associated with capturing techniques and also eliminates the problem of a priori defining a three-dimensional mesh adequate to capture the bow shock within its boundaries. Recently, Shankar[11] has also extended his techniques to include nonconical flows about axisymmetric bodies and they compare favorably with the results of Ref. 4.

Analytically defined geometry is always the first choice, but, unfortunately, is not always available. For practicality, the geometry of Ref. 17, which uses bicubic surface patches, has been included in the present version of the nonlinear code commonly referred to as NCOREL. The current capability of the patch geometry as adapted for use in NCOREL includes body, wing, and wing-body geometries.

The intent of the present study is to apply the methodology of Refs. 4 and 9 to a variety of three-dimensional geometries, where wind tunnel data are available for correlation, to show the accuracy and flexibility of the nonlinear analysis for complex geometries. These geometries include three basic types: arbitrary body, wings, and blended wing-body configurations.

Analytic Forebodies

A series of analytically defined forebodies were tested at supersonic speeds ranging from $M_\infty = 1.70$ to 4.50 and the pressure data is available in Ref. 14. Two of these body shapes were chosen to determine the accuracy of NCOREL with respect to surface pressure data at $M_\infty = 1.70$. All the computations were carried out on a $38 \times 30 \times 50$ mesh, where 38 points were distributed around the body and 50 radial marching steps or $\Delta z/L = 0.02$ were used. The Joukowski mapping was not implemented for these body shapes. The

Presented as Paper 82-0167 at the AIAA 20th Aerospace Sciences Meeting, Orlando, Fla., Jan. 11-14, 1982; submitted Jan. 22, 1982; revision received July 22, 1982.

*Staff Scientist, Research and Development Center.

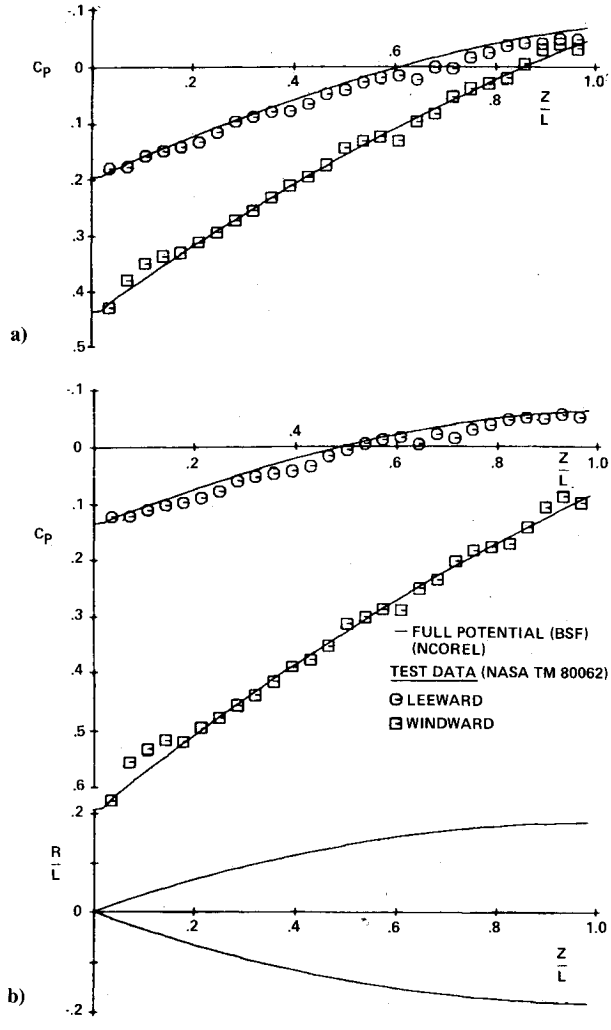

Fig. 1 Axial pressure distribution on a parabolic arc body with lobed cross section at $M_\infty = 1.70$. a) $\alpha = 5.35$ deg. b) $\alpha = 10.35$ deg.

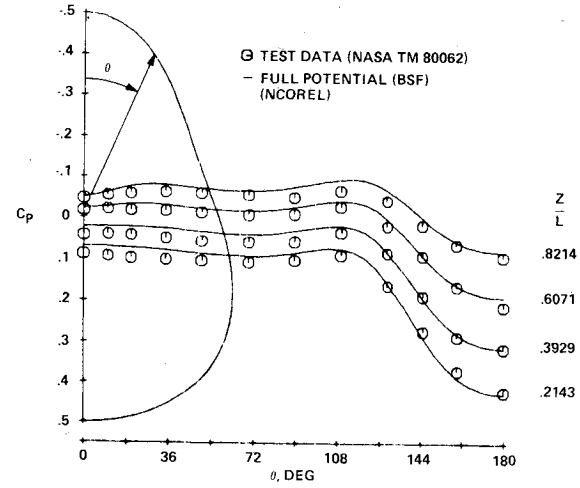

Fig. 2 Azimuthal pressure distribution on a parabolic arc body with lobed cross section, $M_\infty = 1.70$, $\alpha = 10.35$ deg.

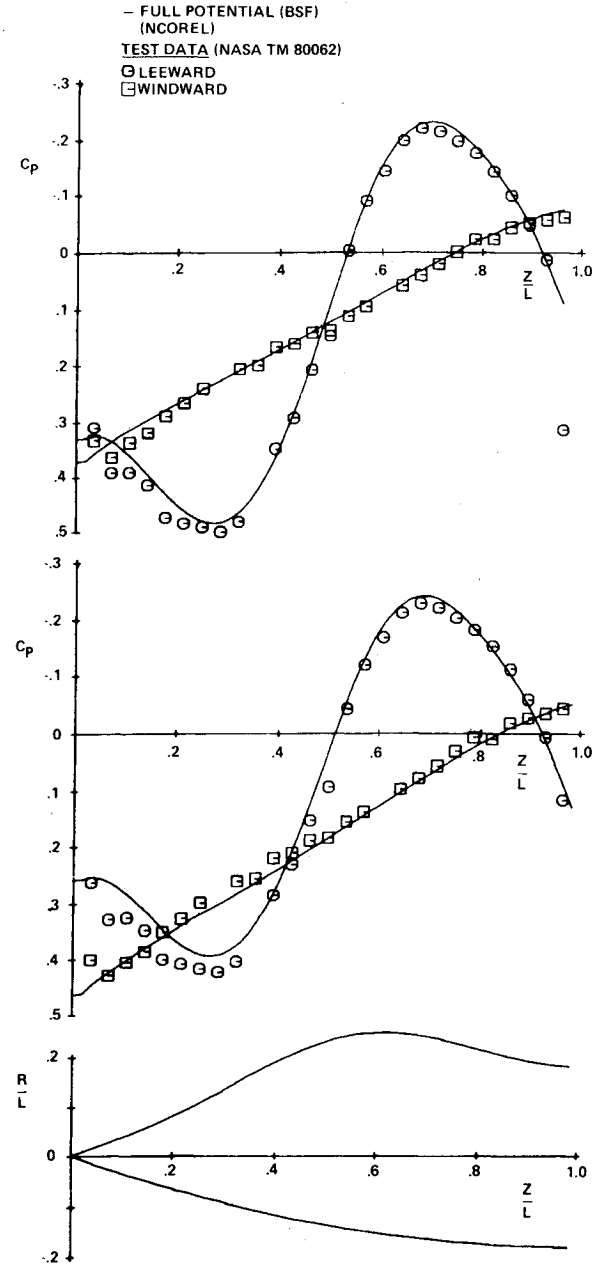

Fig. 3 Axial pressure distribution on a fuselage forebody shape, $M_\infty = 1.70$.

total run times ranged from 4 to 7 min on an IBM 370/168, with the spherical geometry generation requiring approximately 2-3 min of the total run time.

Figures 1a and 1b show the computed windward and leeward symmetry plane pressures compared to the test data at $M_\infty = 1.70$ for a parabolic arc body with a lobed cross section at $\alpha = 5.35$ and 10.35 deg, respectively. The test data do not exhibit a smooth behavior owing to either probe or geometric inaccuracies. Excellent overall comparison is achieved at these angles of attack. Figure 2 shows a comparison of the computed azimuthal pressure distributions with data for the same body at $M_\infty = 1.70$, $\alpha = 10.35$ deg for several axial locations. Excellent agreement in the azimuthal shape of the pressure distribution is achieved with a slight difference in the magnitude of the pressure levels.

Figure 3 shows another set of comparisons for a fuselage forebody shape at $M_\infty = 1.70$, $\alpha = 1.00$ and 5.01 deg. According to Ref. 14, the first five pressure taps were incorrectly located and hence do not necessarily lie on the symmetry planes and should be disregarded. Figure 4 shows the azimuthal pressure distributions for the same body at $M_\infty = 1.70$, $\alpha = 1.00$ deg for several axial locations.

Overall excellent agreement with the test data was achieved.

Analytic Arrow Wing

Reference 15 reports on a series of wind tunnel tests for four analytically defined arrow wings. This experiment was selected because of the availability of detailed spanwise data at several stations for a three-dimensional configuration. The

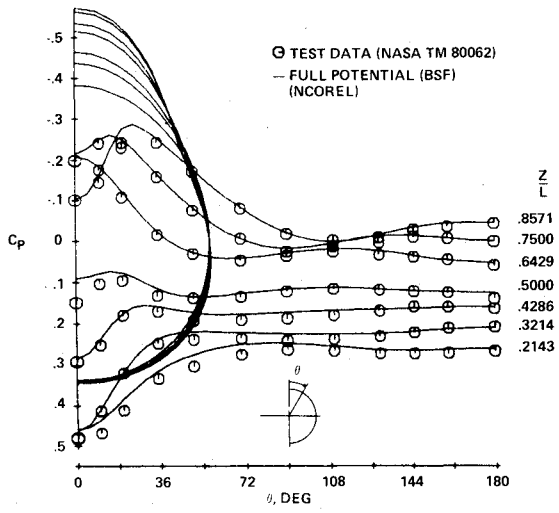

Fig. 4 Azimuthal pressure distribution on a fuselage forebody, $M_\infty = 1.70$, $\alpha = 1$ deg.

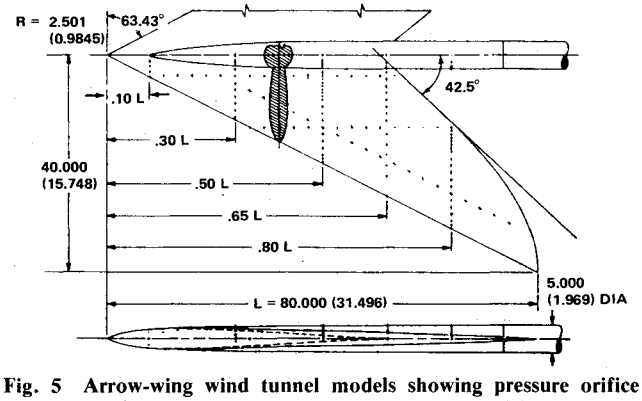

Fig. 5 Arrow-wing wind tunnel models showing pressure orifice locations. Dimensions are in centimeters (inches) (Ref. 15).

basic symmetrical wing configuration referred to as model 1 with a sweep angle $\Lambda = 63.43$ deg was used for the present study (see Fig. 5). The analytical geometry was kindly supplied by G. Moretti of Polytechnic Institute of New York (PINY) in the form of a computer subroutine.

The geometry consists of a wing with a straight leading edge and a circular centerbody emerging from the wing downstream of the apex. The variable sweep trailing edge of the wing remains a supersonic trailing edge for all Mach numbers tested. The geometry was run in NCOREL at the lowest test Mach number of 2.36. A 57×41 cross-flow plane grid and 40 radial steps were used for the computation.

Figure 6 shows the correlation achieved for $\alpha = 6$ deg and span stations $Z/L = 0.30$, 0.50, 0.65, and 0.80. The computed results at a spanwise station were obtained by interpolation of the results from the spherical surfaces. The body has already emerged from the wing at the first span station (Fig. 6a), where $Z/L = 0.30$. The grid definition of the body is adequate at this station. The computed pressures do not indicate any localized spanwise effect due to the wing-body juncture, although the test data show a slight variation in the vicinity of the juncture. A cross-flow shock is not indicated in either the experimental data or the computed results at this station. Figures 6b and 6c show two further downstream stations. The formation of a weak cross-flow shock is now evident. At these stations the grid definition of the body is rather poor yet the correlation in pressures remains excellent. Figure 6d shows a station downstream of the trailing edge of the wing. No attempts were made to actually compute the wake. Instead, a flat plate approximation for the wake was used to indicate the type of results that could be achieved with this crude approximation. Since the trailing edge is supersonic, the inviscid solution on the wing surface should not be influenced by the wake approximation. Remarkably good comparison is achieved on the wing surface using this approximation. The computed results indicate trailing-edge shocks which occur because of the supersonic nature of the trailing edge. The local solution for the shocks in the vicinity of the trailing edge is not good because of the erroneous flat plate approximation as well as boundary-layer effects and artificial smearing of the oblique trailing-edge shocks. Smearing of the trailing-edge shocks occurs because grid points are not necessarily located on the exact trailing edge of the wing and also owing to the use of numerical central difference formulas for the computation of body spanwise slopes. The computed body pressures do not correlate with the test data. This was expected because the wake of the wing has a definite influence on the body, unlike on the wing. Some difficulty in the geometry of the flat plate wake occurred, as indicated in Fig. 6d by the wake crossover.

The computed results have a tendency to slightly underpredict the supercritical pressures and indicate a slightly downstream position of the cross-flow shock in comparison with the test data. This discrepancy may in part be due to the rotational effects associated with the high Mach number of 2.36 which are neglected in the present potential theory.

Higher angles of attack were not computed because the experimental pressure distributions indicated a flat leeward pressure distribution with the absence of a cross-flow shock. This is generally indicative of leeward surface boundary-layer separation and correlation with inviscid solutions would not be expected.

Supersonic Cruise Aircraft

A more stringent test of the code in computing wing-body geometries is the type of configuration where the body origin lies upstream of the wing origin which is typical of any realistic aircraft. This type of geometry leads to the formation of an embedded oblique wing shock. Reference 16 contains spanwise surface pressure data for a supersonic cruise aircraft configuration at Mach numbers 2.30, 2.96, and 3.30. Reference 16 was chosen because it also contains detailed measured geometric data of the complete aircraft in the form of an input data set consistent with the patch geometry requirements of Ref. 17.

Figure 7 shows the panel definition of the aircraft and the location of some of the pressure stations used for comparison defined in aircraft model coordinates (in inches). The geometry data set of Ref. 16 was modified for use in NCOREL. The engine nacelles and vertical tails were removed. The wing model contains a total of 650 panels and the fuselage model, which was made simpler than that of Ref. 16, contains a total of 328 panels. The Joukowski mapping singularity was then tied to the evolution of the wing. Hence, the mapping singularity remains on the axis of the aircraft until the wing origin, the singularity then moves continuously outward with the wing as the wing emerges from the fuselage. This procedure was found to be necessary because abrupt changes in singularity location cause abrupt changes in the mesh and lead to erroneous results. The camber of the wing centerline section was also modified to make the apex of the wing coincide with the origin of the fuselage so that the mapping singularity smoothly departs from the origin of the fuselage.

Some preliminary computations were carried out at $M_\infty = 2.30$. A 58×58 cross-sectional mesh was used with a marching step size of $\Delta Z = 2$ which yielded approximately 23 steps to the centerline trailing edge of the wing. Figure 8 shows an isometric plot of the spanwise cross sections and pressure distributions at $M_\infty = 2.30$, $\alpha = 4.82$ deg. As noted earlier, the numerical program marches on spherical surfaces using the spherical cross-sectional geometry. Figure 8 was obtained from the spherical data by linear interpolation. A large low-pressure spike occurs as the wing emerges from the

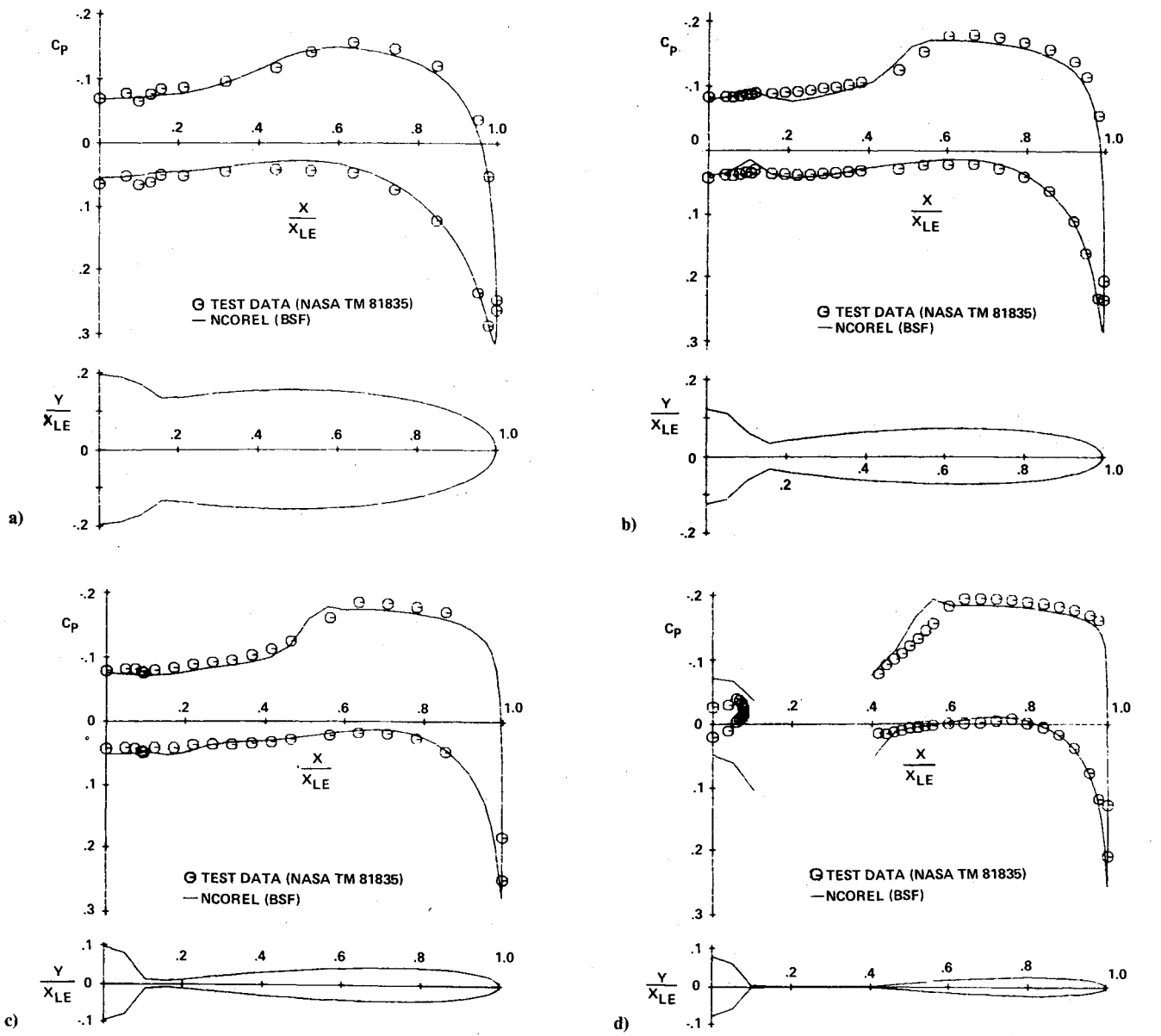

Fig. 6 Spanwise pressure distribution on an analytically defined arrow wing, $M_\infty = 2.36$, $\alpha = 6$ deg. a) $Z/L = 0.30$. b) $Z/L = 0.50$. c) $Z/L = 0.65$. d) $Z/L = 0.80$.

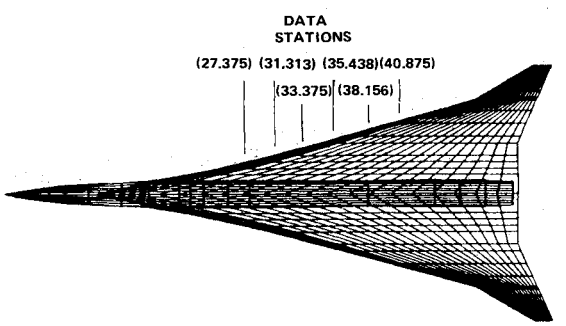

Fig. 7 Input panel model of supersonic cruise aircraft showing pressure data stations used for comparison.

fuselage ($\Delta x \simeq 14$). The spike remains throughout and a cross-flow shock quickly develops. Interesting to note is the pressure depression that occurs due to the fuselage. Just after the wing emerges, the pressure distribution exhibits large oscillations on the leeward surface, causing convergence problems. This may be related to oscillations in the geometry or, perhaps, to the simultaneous development of the oblique embedded wing shock due to the wing emergence from the fuselage and the appearance of the supercritical cross-flow shock.

If a thin wing (i.e., in comparison to the fuselage) emerges from the fuselage a new scale to the problem is created. In the wing-body calculation, only a few points will be distributed between the newly emerged wing surface and oblique wing shock embedded in the fuselage flowfield. As the oblique wing shock moves away from the wing surface towards the bow shock, the resolution becomes better. It is suspected that this is the primary difficulty being encountered in the vicinity of the wing emergence from the fuselage. The lack of resolution can create oscillations and convergence problems, especially if a supercritical region has developed. A stretching of the coordinates creating a cluster near the newly emerged wing surface may be necessary to alleviate this problem.

The computed results show a large suction spike at the leading edge with a steep adverse pressure gradient. The computed solution indicates that the suction spike induces a cross-flow shock. The flow then expands slightly to further recompress through a second cross-flow shock. This unusual behavior is most probably caused by the small nose radius and rather large camber. The suction spike would most probably

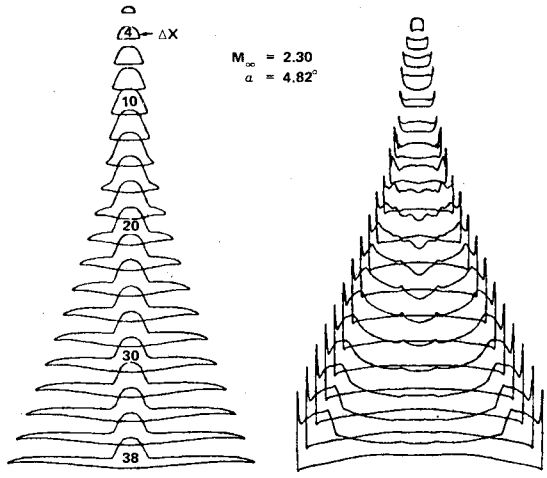

Fig. 8 Isometric view of spanwise cross sections and pressure distributions ($\Delta X = 2$).

cause the leading edge to separate. Figure 9 shows a series of comparisons at $M_\infty = 2.30$ and $\alpha = 4.82$ deg between a wing-body and wing-alone calculation with the corresponding test data. The presence of the body has a minor effect on the windward pressures and a significant but local effect on the leeward surface, yielding a compression from the wing-body juncture to the centerline. Both wing and wing-body calculations exhibit leading-edge suction spikes, with the wing-body exhibiting a more inward location and a slightly stronger cross-flow shock. Overall the two calculations compare favorably with only minor and expected differences.

The leeward surface experimental pressure data do not indicate a suction spike or a cross-flow shock. The absence of a cross-flow shock in the experimental data as the wing becomes thinner must be due to leading-edge boundary-layer separation.

The lack of correlation in the leeward surface pressures led to a closer inspection of the test data. Two intermediate stations where only leeward pressure data points were taken are plotted for comparison in Figs. 10a and 10b for $\alpha = 2.81$ and 4.82 deg without the wing-alone solutions. Remarkably good correlation was achieved with the leeward pressures at these two intermediate stations. Interesting to note is that the two intermediate stations exhibit cross-flow shocks at the higher angle of attack ($\alpha = 4.82$ deg). Also, if one compares the station of Fig. 10 with the stations shown in Fig. 9, the experimental leeward data of the two intermediate stations are distinctly different from their neighboring stations.

Unfortunately, there is no way of knowing how much leading-edge separation is occurring or the reliability and accuracy of the test data, given the strange behavior for the leeward surface pressures. This is always the case when a configuration has been tested without prior nonlinear analysis. In the future, three-dimensional wings and wing-bodies will be designed with the nonlinear analysis codes to prevent or minimize leading-edge separation and, we hope, more fully validate the nonlinear analysis in the wind tunnel. One such test will be conducted in the near future at NASA Langley for a realistic three-dimensional wing.

Zero-Lift Wave Drag

Figure 11 shows a series of numerical computations at several Mach numbers for a three-dimensional delta wing ($\Lambda = 71.57$ deg) at 0 angle of attack. The Weber version (see Ref. 18) of the Squire delta wing has a circular arc centerline thickness distribution with elliptic spanwise cross sections. To compute the entire wing in a spherical coordinate system, a flat plate was inserted for the wake geometry. This is a valid approximation since the wing is symmetric and at 0 angle of attack. The computed pressures on the wing were integrated

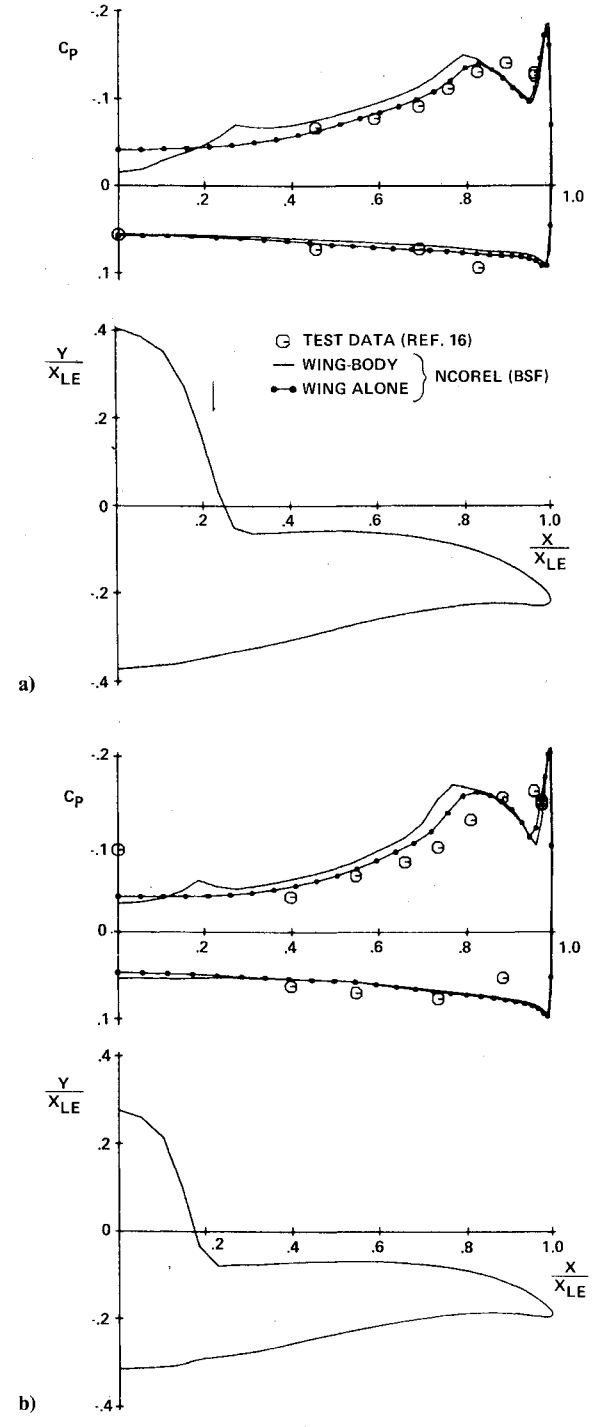

Fig. 9 Comparison of computed wing-alone and wing-body configurations with pressure data for $M_\infty = 2.30$, $\alpha = 4.82$ deg. a) Station 31.313. b) Station 35.438.

to obtain the zero-lift wave drag values at several different Mach numbers and were compared to experimental values and the Squire linearized analysis. This computation was suggested by Mason because it had been noted earlier in Ref. 5 that linearized theory has a tendency to overpredict the drag. Hence the opportunity exists of achieving lower levels of drag using a more accurate nonlinear analysis tool. The nonlinear code shows a marked improvement above Mach 1.8 for the difficult prediction of zero-lift wave drag. The discrepancies at the lower Mach numbers are being investigated. At the Mach numbers 1.5 and 1.6, the linearized results show slightly better agreement. The accuracy of the nonlinear analysis depends upon the accuracy of capturing the oblique trailing-edge shocks. To better resolve these shocks, a windward

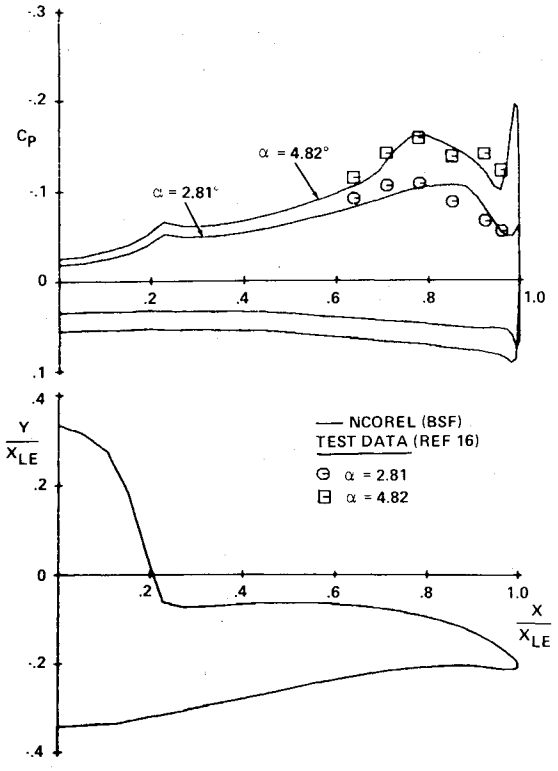

a)

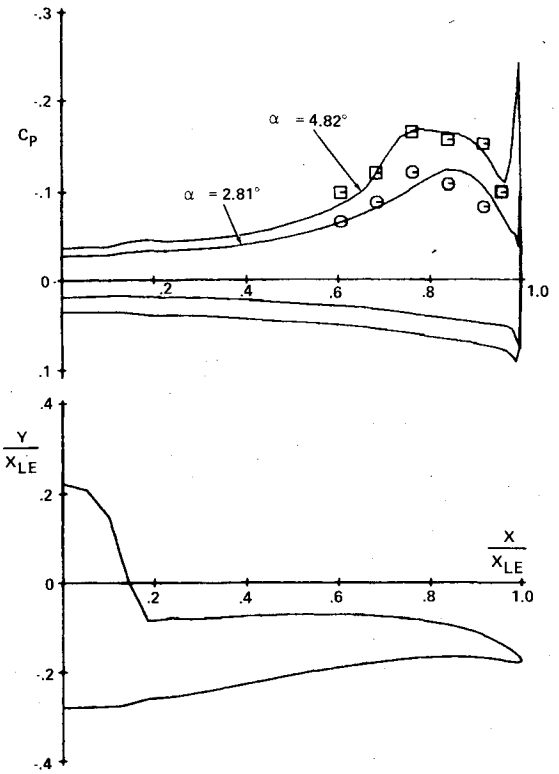

b)

Fig. 10 Comparison with surface pressure data for a supersonic cruise aircraft at $M_\infty = 2.30$, $\alpha = 2.81$ and 4.82 deg. a) Station 33.375. b) Station 38.156.

differencing was used to determine the numerical surface slopes in the radial marching direction. Less smearing of these shocks occurred when this was done and slightly better correlation was achieved. No attempts were made in the nonlinear analysis to actually delineate the trailing edge of the wing. Aft of the trailing edge the spherical cross sections take on a lobed appearance outboard of the wake region. A grid point on the body surface did not necessarily fall exactly on

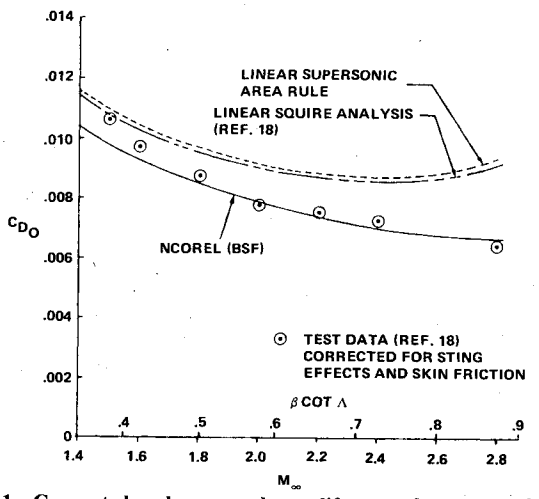

Fig. 11 Computed and measured zero-lift wave drag on the Squire delta wing.

the trailing edge of the wing. Also, centered differences were used to determine the circumferential body slopes. All of this tends to artificially smear the oblique trailing-edge shock. The surface pressures on the wing should not be influenced by the trailing-edge shocks, but, unfortunately, the above numerical approximations that tend to smear the trailing edge affect the wing pressures slightly. In the future, numerical calculations will be performed where the trailing edge of the wing will be defined in the code to facilitate the proper differencing to accurately capture the oblique trailing-edge shocks.

Conclusions

A nonlinear supersonic analysis code (NCOREL) has been developed for computing inviscid flows over arbitrary bodies, wings, and wing-body configurations. The code has been shown to be extremely successful in computing arbitrary bodies and blunt leading-edge wings.

Preliminary calculations using aerodynamic input data and point body definition with spline and bicubic surface patch fitting for the geometry has been carried out on a realistic wing-body configuration. Varying degrees of correlation were achieved. Inconsistencies in the leeward pressure data were apparent, causing one to suspect the accuracy or validity of the test data and geometric input.

The additional scale to the problem, generated by the newly emerged wing, causes resolution difficulties. This may be resolved in the future by including a stretching that clusters grid points near the wing surface as the wing emerges from the fuselage.

The zero-lift wave drag was computed on a delta wing with an elliptical cross section by integration of the numerical pressure data. Excellent agreement with measured data was obtained between $M_\infty = 1.8$ and 2.8, showing a marked improvement over analytical and numerical linearized analyses. Some discrepancy occurred in the lower Mach number range near $M_\infty = 1.5$. Trailing-edge shock smearing may be partly responsible for this discrepancy. A more accurate treatment of the wing trailing edge and wake will be investigated in future applications.

Acknowledgment

This work was partially funded by NASA Langley Research Center under Contract NAS 1-16758.

References

[1]Brown, C., McLean, F., and Klunker, E., "Theoretical and Experimental Studies of Cambered and Twisted Wings Optimized for Flights at Supersonic Speeds," *Proceedings of the 2nd International Congress of Aerospace Sciences, Advances in Aerospace Sciences,*

Vol. 3, edited by T. von Karman et al., Pergamon Press, Oxford, 1962.

[2]Marconi, F. and Siclari, M.J., "A Study of the Inviscid Flow About Conically Cambered Delta Wings," AIAA Paper 78-58, Jan. 1978.

[3]Grossman, B., "Numerical Procedure for the Computation of Irrotational Conical Flows," *AIAA Journal,* Vol. 17, Aug. 1979, pp. 828-837.

[4]Grossman, B. and Siclari, M.J., "The Nonlinear Supersonic Potential Flow Over Delta Wings," AIAA Paper 80-0269, Jan. 1980.

[5]Mason, W.H. and daForno, G., "Opportunities for Supersonic Performance Gains Through Non-Linear Aerodynamics," AIAA Paper 79-1527, July 1979.

[6]Siclari, M.J., "Investigation of Cross Flow Shocks on Delta Wings in Supersonic Flows," *AIAA Journal,* Vol. 18, Jan. 1980, p. 85.

[7]Carmichael, R.L. and Erickson, L.L., "Pan Air—A Higher Order Panel Method for Predicting Subsonic or Supersonic Linear Potential Flows About Arbitrary Configurations," AIAA Paper 81-1255, 1981.

[8]Siclari, M.J., Marconi, F., and Grossman, B., "Analysis and Design of Supersonic Aircraft Based on Inviscid Nonlinear Eulerian Equations," AFWAL TRE-80-3110, Parts I and II, Oct. 1980.

[9]Siclari, M.J., "Supersonic Nonlinear Potential Flows with Subsonic Regions and Implicit Isentropic Shock Fitting," AIAA Paper 81-1201, June 1981.

[10]Shankar, V. and Chakravarthy, S., "An Implicit Procedure for the Treatment of Supersonic Flow Fields Using Conservative Full Potential Equation," *Proceedings of the AIAA Computational Fluid Dynamics Conference,* Palo Alto, Calif., June 1981, pp. 90-100.

[11]Shankar, V., "Treatment of Conical and Nonconical Supersonic Flows by an Implicit Marching Scheme Applied to the Full Potential Equation," *ASME Computers in Flow Predictions and Fluid Dynamics Experiments.* Nov. 1981.

[12]Jameson, A., "Iterative Solution of Transonic Flow over Airfoils and Wings, Including Flows at Mach 1," *Communications on Pure Applied Mathematics,* Vol. 27, May 1974, pp. 283, 309.

[13]Mason, W.H., "Experimental Pressure Distributions and Aerodynamic Characteristics of a Flat Wing and a Cambered Wing Designed for High Lift Coefficients at $M=1.62$," Grumman Test Data Report, Aerodynamics Report 393-79-01, Grumman Aerospace Corp., Bethpage, N.Y., Dec. 1979.

[14]Townsend, J.C., Howell, D.T., Collins, I.K., and Hayes, C., "Surface Pressure Data on a Series of Analytic Forebodies at Mach Numbers from 1.70 to 4.50 and Combined Angles of Attack and Sideslip," NASA TM 80062, June 1979.

[15]Townsend, J.C., "Pressure Data for Four Analytically Defined Arrow Wings in Supersonic Flow," NASA TM 81835, Sept. 1980.

[16]Shrout, B.L., Corlett, W.A., and Collins, I.K., "Surface Pressure Data for a Supersonic-Cruise Airplane Configuration at Mach Numbers of 2.30, 2.96, and 3.30," NASA TM 80061, May 1979.

[17]Craidon, C.B., "A Computer Program for Fitting Smooth Surfaces to an Aircraft Configuration and Other Three Dimensional Geometries," NASA TMX 3206, June 1975.

[18]Weber, J. and King, C., "Analysis of the Zero-Lift Drag Measured on Delta Wings," ARC R&M 3818, June 1976.